Theoretical Uncertainty in the Classification Setpoint of the Aerodynamic Aerosol Classifier: v2

J.P.R. Symonds, Cambustion

18th September 2023

1 Introduction

The Aerodynamic Aerosol Classifier (AAC, Tavakoli & Olfert (2013), Tavakoli et al. (2014)) classifies particles by their relaxation time (τ, directly related to aerodynamic diameter, d_a, by equation 7 below). Particles enter a sheath flow of clean air in a rotating classifier, and the effect of the drag of the particles in the sheath flow (their mobility) and the centrifugal force acting on the mass of the particles means that only those in a narrow range of mass to drag ratio (or relaxation time) emerge through a narrow exit channel.

Some studies have tried to experimentally quantify the uncertainty in measurement of diameter with the commercially available AAC by using standard polystyrene-latex (PSL) spheres. Johnson et al. (2018) showed agreement with PSL size when step-scanning the AAC to be within 4.7%. Johnson et al. (2021) showed that when continuously scanning an AAC the agreement was within 8.7% of the stated PSL particle sizes, or 5.7% if the uncertainty in the stated sizes is considered. Such work is however always subject to experimental uncertainty, and whilst such spheres are certified for their "true" spherical diameter, knowledge of their density is also required to know their aerodynamic diameter. The density of PSL is generally not certified, and the density (and indeed size) of the nebulised, dried spheres is subject to being affected by impurities in the fluid they are suspended in.

Here we undertake a simple uncertainty propagation analysis of the AAC. The relaxation time is considered first, as this is purely and simply a function of the sheath flow rate, the rotational speed, and the classifier dimensions; therefore it can be looked at purely analytically. We then consider the conversion of relaxation time to aerodynamic diameter, which as it involves the empirically derived and non-linear Cunningham slip correction factor, requires some numerical analysis. Conversion to aerodynamic diameter also involves considering the mean free path and viscosity of the carrier gas, which are in turn functions of both the ambient temperature and pressure, and just ambient temperature, respectively.

Finally, we attempt a better estimate of the uncertainties in the rotational speed and sheath flow, based on field calibration data from real AACs, and use this to further refine the overall uncertainty.

2 Uncertainty in relaxation time

The fundamental expression (Tavakoli & Olfert 2013) for the set-point of the AAC is

$$\tau^* = \frac{2Q_{\mathrm{sh}}}{\pi\omega^2 \left(r_1 + r_2\right)^2 L} \tag{1}$$

where τ^* is the peak of the transfer function in terms of relaxation time, Q_{sh} is the sheath flow, ω is the rotational speed, r_1 and r_2 are the radii of the cylinders and L is the effective length of the classifier, inlet to outlet. The variance formula for the propagation of uncertainties gives

$$\sigma_\tau^2 = \left(\frac{\partial\tau}{\partial Q_{\mathrm{sh}}}\right)^2 \sigma_Q^2 + \left(\frac{\partial\tau}{\partial\omega}\right)^2 \sigma_\omega^2 + \left(\frac{\partial\tau}{\partial L}\right)^2 \sigma_L^2 + \left(\frac{\partial\tau}{\partial r_1}\right)^2 \sigma_{r_1}^2 + \left(\frac{\partial\tau}{\partial r_2}\right)^2 \sigma_{r_2}^2. \tag{2}$$

Evaluating the partial derivatives, substituting back in for τ and re-arranging to give fractional uncertainty gives

$$\left(\frac{\sigma_\tau}{\tau}\right)^2 = \left(\frac{\sigma_Q}{Q_{\mathrm{sh}}}\right)^2 + \left(\frac{2\sigma_\omega}{\omega}\right)^2 + \left(\frac{\sigma_L}{L}\right)^2 + 2\left(\frac{2\sigma_r}{r_1 + r_2}\right)^2, \tag{3}$$

where it assumed $\sigma_{r_1} = \sigma_{r_2} = \sigma_r$.

We now consider each of these terms in turn. ISO15900:2009 (ISO 2009) suggests the uncertainty for the sheath flow in a Differential Mobility Analyser (DMA) to be 0.06 lpm on a 3.00 lpm flow, or 2%. This seems like a fair figure to use here.

Symonds et al. (2013) give the uncertainty in the Centrifugal Particle Mass Analyser (CPMA) speed to be 0.5% — the AAC uses the same motor and controller so this seems fair to use here too for σ_ω/ω.

Though the machining tolerance of the inlet and outlet on the AAC is much better than this, let us assume a 1 mm tolerance on the length. This is because the effective length of the classifier (206 mm) also depends to an extent on wider geometry and exact flow patterns. This is perhaps the "most uncertain of the uncertainties". This is similar to the 0.5% uncertainty which ISO (2009) suggests for the length of a DMA column.

The cylinders themselves (of 56 mm and 60 mm radii) are manufactured to a tolerance in diameter of 50 microns, or 25 microns in radius (Symonds 2023).

Altogether this gives:

$$\left(\frac{\sigma_\tau}{\tau}\right)^2 = 0.02^2 + (2 \times 0.005)^2 + \left(\frac{1}{206}\right)^2 + 2 \times \left(\frac{2 \times 0.025}{56 + 60}\right)^2 \quad (4)$$

$$= 0.004 + 0.0001 + 2.36 \times 10^{-5} + 3.71 \times 10^{-7} \quad (5)$$

$$\frac{\sigma_\tau}{\tau} = 2.3\% \quad (6)$$

with the majority of the uncertainty coming from the sheath flow, followed by the speed, followed by the length and (much further down the line) the radii.

3 Uncertainty in aerodynamic diameter

The relationship between τ and d_a is

$$\tau = \frac{C_\mathrm{C}(d_\mathrm{a})\rho_0 d_\mathrm{a}^2}{18\mu} \quad (7)$$

where C_C is the Cunningham slip correction, μ is the viscosity of the gas and $\rho_0 \equiv 1000$ kg m^{-3}. Both C_C and μ will have uncertainties. The latter depends upon the temperature of the gas. The former not only depends on the mean free path of the gas (which in turn is a function of temperature and pressure) and d_a itself, it is also subject to the inherent uncertainty in the empirically derived slip correction expression, which has a number of varying forms in the literature. It is beyond the scope of this report to go into uncertainties in the slip correction and ambient conditions. We instead concentrate on the relationship between the uncertainty in τ and that of d_a — this is inherently size dependant as C_C is size dependant.

The form of the slip correction used by the AAC software is that of Kim et al. (2005):

$$C_\mathrm{C} = 1 + \frac{2l}{d}\left[A + B\exp\left(-\frac{Cd}{2l}\right)\right] \quad (8)$$

where empirical constants $A = 1.165$, $B = 0.483$ and $C = 0.997$ and l is the mean free path of the gas.

At large particle sizes, slip correction is no longer necessary, the second term tends to 0 and hence $C_\mathrm{C} \to 1$. In this case, $\tau \propto d_\mathrm{a}^2$ and

$$\lim_{d_\mathrm{a}\to\infty}\left(2\frac{\sigma_d}{d_\mathrm{a}}\right)^2 = \left(\frac{\sigma_\tau}{\tau}\right) \quad (9)$$

$$\lim_{d_\mathrm{a}\to\infty}\frac{\sigma_d}{d_\mathrm{a}} = {}^1\!/_2\frac{\sigma_\tau}{\tau} = 1.2\%. \quad (10)$$

At small particle sizes, the $[(2l/d)\cdot A]$ term dominates (as the exponential term tends to zero) so $C_\mathrm{C} \to 2lA/d$. In this case $\tau \propto d_\mathrm{a}$ and

$$\lim_{d_\mathrm{a}\to 0}\left(\frac{\sigma_d}{d_\mathrm{a}}\right)^2 = \left(\frac{\sigma_\tau}{\tau}\right)^2 \quad (11)$$

$$\lim_{d_\mathrm{a}\to 0} \frac{\sigma_d}{d_\mathrm{a}} = \frac{\sigma_\tau}{\tau} = 2.3\%. \tag{12}$$

In the general case

$$\frac{\sigma_d}{d_\mathrm{a}} = \frac{\sigma_\tau}{\tau} \cdot \left.\frac{\partial d_\mathrm{a}}{\partial \tau}\right|_{d_\mathrm{a}} \cdot \frac{\tau}{d_\mathrm{a}} = 2.3\% \times \left.\frac{\partial d_\mathrm{a}}{\partial \tau}\right|_{d_\mathrm{a}} \cdot \frac{\tau}{d_\mathrm{a}}. \tag{13}$$

So for ambient conditions of 25° C and 1 atm, we numerically differentiate equation 7 to give the $(\partial d_\mathrm{a}/\partial\tau)|_{d_\mathrm{a}}$ term and hence we can plot σ_d/d_a and σ_d as a function of d_a over the full size range of the AAC as Figure 1.

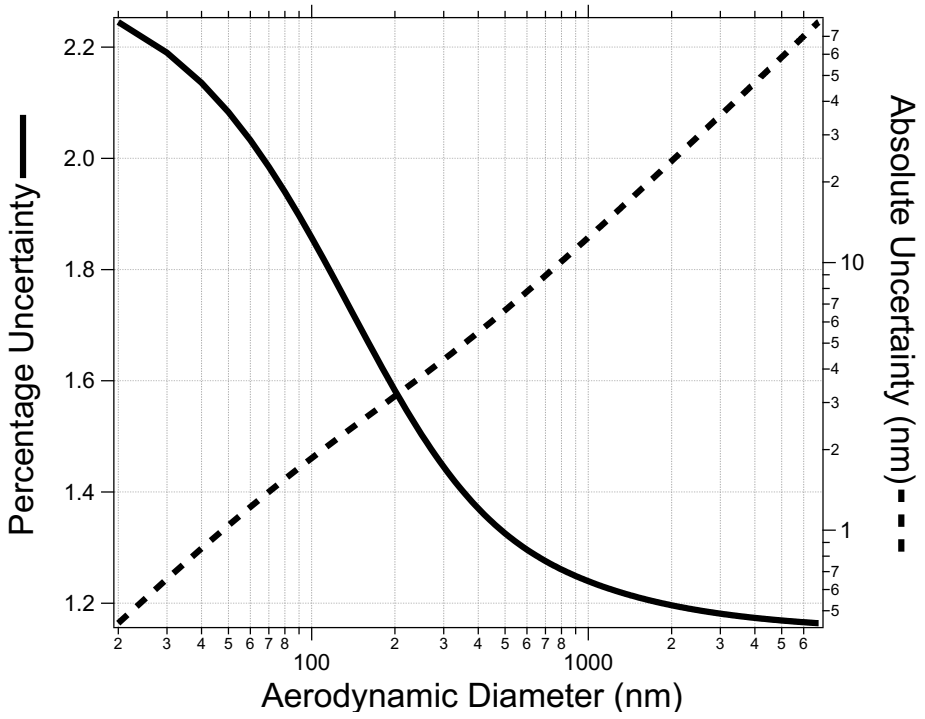

Figure 1: Uncertainty in d_a (excluding uncertainty in gas T, p)

4 Considering uncertainty in temperature and pressure

$$\sigma_d^2 = \left(\frac{\partial d_\mathrm{a}}{\partial \tau}\right)^2 \sigma_\tau^2 + \left(\frac{\partial d_\mathrm{a}}{\partial T}\right)^2 \sigma_T^2 + \left(\frac{\partial d_\mathrm{a}}{\partial p}\right)^2 \sigma_p^2 \tag{14}$$

$$\left(\frac{\sigma_d}{d_\mathrm{a}}\right)^2 = \left(\frac{\partial d_\mathrm{a}}{\partial \tau}\frac{\sigma_\tau}{d_\mathrm{a}}\right)^2 + \left(\frac{\partial d_\mathrm{a}}{\partial T}\frac{\sigma_T}{d_\mathrm{a}}\right)^2 + \left(\frac{\partial d_\mathrm{a}}{\partial p}\frac{\sigma_p}{d_\mathrm{a}}\right)^2 \tag{15}$$

$$\left(\frac{\sigma_d}{d_\mathrm{a}}\right)^2 = \left(\frac{\partial d_\mathrm{a}}{\partial \tau}\frac{\sigma_\tau}{\tau}\frac{\tau}{d_\mathrm{a}}\right)^2 + \left(\frac{\partial d_\mathrm{a}}{\partial \tau}\frac{\partial \tau}{\partial T}\frac{\sigma_T}{d_\mathrm{a}}\right)^2 + \left(\frac{\partial d_\mathrm{a}}{\partial \tau}\frac{\partial \tau}{\partial p}\frac{\sigma_p}{d_\mathrm{a}}\right)^2 \tag{16}$$

The pressure sensor used to rated to be accurate to within 1% of full scale, and K-type thermocouples are known to be accurate to within 2.2°C (ASTM 2017) at room temperature. The thermocouple reading IC is rated to be within 2°C, so combining these two sources of error in temperature, the uncertainty in temperature is taken to be 3 °C.

We evaluate the differentials numerically and the result is given as figure 2. The contribution from the uncertainty in pressure and temperature are each

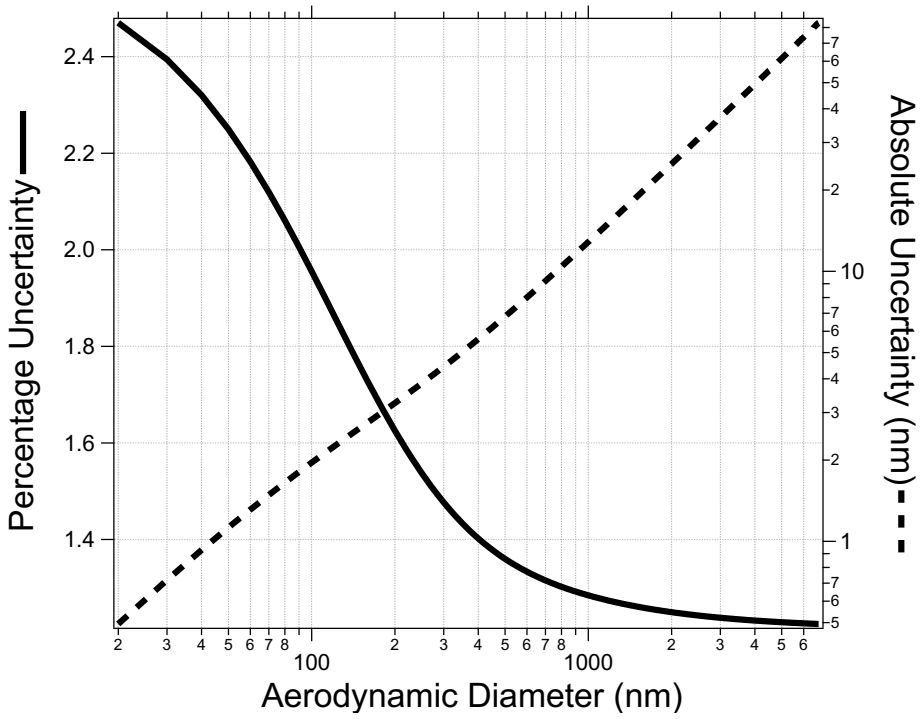

Figure 2: Uncertainty in d_a (including uncertainty in gas T, p)

between a factor of ⅓ and 2 orders of magnitude lower than that from the relaxation time.

None of this takes into account the uncertainty in the mathematical form of the slip correction, which is of course itself empirically derived and subject to uncertainty.

5 Uncertainty in speed and sheath flow from field calibration data

Every AAC which is sold new or serviced has its rotational speed and sheath flow checked against traceable standards. The volumetric sheath flow values are checked against a Sensidyne Gilibrator bubble-cell flowmeter, and the rotational speed against a Compact Instruments laser tachometer. Cambustion reports the difference between the AAC's readings and the two standards on the calibration report sent with each instrument.

Let's assume the errors in the standards themselves are random and normally distributed with a standard deviation equal to the manufacturer's reported accuracy. We add a random error calculated on this basis to the recorded difference to the standard for each AAC to give a total error "from the truth" for that AAC. We take the mean of those absolute percentage errors across all AACs, and repeat the above a number of times with different random errors in the standards, and obtain a mean of the means as an estimate of the overall uncertainty in that quantity. The table below gives the manufactures reported accuracy of the standards, the mean absolute percentage difference to the standards amongst all AACs, and the final estimate of the uncertainty, for each quantity.

Quantity	Quoted accuracy of calibration standard	Mean absolute difference to standard	Final uncertainty estimate
Sheath Flow (Q_{sh})	±1.0%	0.70%	1.04%
Rotational Speed (ω)	±0.5%	0.36%	0.55%

Putting these values into equation 3 along with the same geometrical uncertainties used above gives the following uncertainty in relaxation time:

$$\left(\frac{\sigma_\tau}{\tau}\right)^2 = 0.0104^2 + (2 \times 0.0055)^2 + \left(\frac{1}{206}\right)^2 + 2 \times \left(\frac{2 \times 0.025}{56+60}\right)^2 \tag{17}$$

$$= 1.08 \times 10^{-3} + 1.21 \times 10^{-3} + 2.36 \times 10^{-5} + 3.71 \times 10^{-7} \tag{18}$$

$$\frac{\sigma_\tau}{\tau} = 1.6\% \tag{19}$$

Note that the speed term is now marginally the largest term. Using this 1.6% value for σ_τ/τ in equation 16, and the methodology in section 4 (including uncertainties in temperature and pressure as given above), produces the plot in figure 3.

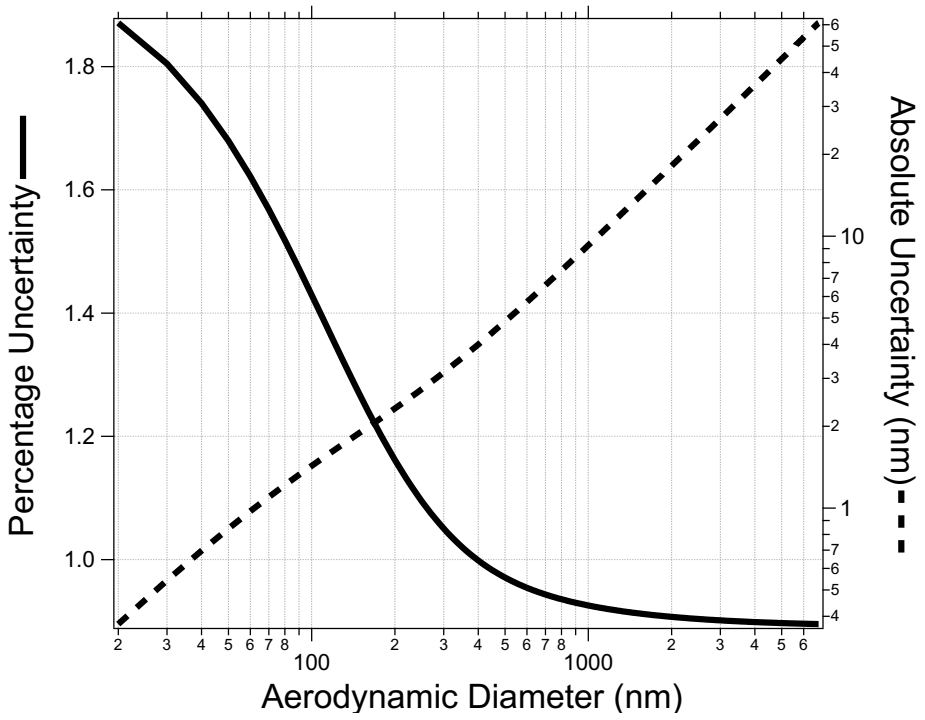

Figure 3: Uncertainty in d_{a} using estimated uncertainties in speed and sheath flow based on field calibration data

References

ASTM (2017), Standard specification for temperature-electromotive force tables for standardized thermocouples, International standard, ASTM International.

ISO (2009), ISO 15900:2009: Determination of particle size distribution — differential electrical mobility analysis for aerosol particles, International standard, International Standards Organisation.

Johnson, T. J., Nishida, R., Irwin, M., Symonds, J. P., Olfert, J. S. & Boies, A. (2018), Agreement between different aerosol classifiers using spherical particles, *in* 'Cambridge Particle Meeting'.

Johnson, T. J., Symonds, J. P. R., Olfert, J. S. & Boies, A. M. (2021), 'Accelerated measurements of aerosol size distributions by continuously scanning the aerodynamic aerosol classifier', *Aerosol Science and Technology* **55**, 119–141.

Kim, J. H., Mulholland, G. W., Kukuck, S. R. & Pui, D. Y. H. (2005), 'Slip correction measurements of certified PSL nanoparticles using a nanometer differential mobility analyzer (nano-DMA) for knudsen number from 0.5 to 83.', *Journal of research of the National Institute of Standards and Technology* **110**, 31–54.

Symonds, J. (2023), 'Cambustion, personal communication'.

Symonds, J. P. R., Reavell, K. S. J. & Olfert, J. S. (2013), 'The CPMA-electrometer system—a suspended particle mass concentration standard', *Aerosol Science and Technology* **47**, i–iv.

Tavakoli, F. & Olfert, J. S. (2013), 'An instrument for the classification of aerosols by particle relaxation time: Theoretical models of the aerodynamic aerosol classifier', *Aerosol Science and Technology* **47**, 916–926.

Tavakoli, F., Symonds, J. P. R. & Olfert, J. S. (2014), 'Generation of a monodisperse size-classified aerosol independent of particle charge', *Aerosol Science and Technology* **48**, i–iv.